Identifying charge and mass transfer resistances of an oxygen reducing biocathode

Annemiek Ter Heijne, Olivier Schaetzle, Sixto Gimenez, Francisco Fabregat-Santiago, Juan Bisquert, David P. B. T. B Strik, Frédéric Barrière, Cees J. N Buisman, Hubertus V. M. Hamelers

HAL Id: hal-00658390

https://hal.archives-ouvertes.fr/hal-00658390

Submitted on 15 Jul 2013

PAPER

Identifying charge and mass transfer resistances of an oxygen reducing biocathode

Annemiek Ter Heijne,[ab] Olivier Schaetzle,[bc] Sixto Gimenez,[d] Francisco Fabregat-Santiago,[d] Juan Bisquert,*[d] David P. B. T. B. Strik,[a] Frédéric Barrière,[c] Cees J. N. Buisman[ab] and Hubertus V. M. Hamelers*[a]

In this study, we identified mass and charge transfer resistances for an oxygen reducing biocathode in a microbial fuel cell (MFC) by electrochemical impedance spectroscopy (EIS). The oxygen reducing biocathode was grown using nitrifying sludge as the inoculum. A standard model for charge transfer at the electrode surface combined with diffusion across a boundary layer was used. EIS measurements were performed under variation of both linear flow velocities and cathode potentials. Fitting the impedance data to the standard model at constant potential and different flow rates confirmed that increasing flow rate had no effect on charge transfer resistance, but led to a decrease in mass transfer resistance. From the variation in cathode potential at constant flow rate, a minimum in charge transfer resistance was found at 0.28 V *vs.* Ag/AgCl. The minimum in charge transfer resistance could be explained by the combined biochemical and electrochemical kinetics typical for bioelectrochemical systems.

1. Introduction

Microbial fuel cells (MFCs) constitute an emerging technology for the production of renewable electricity from biodegradable organic materials.[1] In an MFC, microorganisms catalyze the

[a]Sub-department of Environmental Technology, Wageningen University, Bornse Weilanden 9, P.O. Box 17, 6700 AA Wageningen, The Netherlands. E-mail: Bert.Hamelers@wur.nl; Fax: +31-317-482108; Tel: +321-317-483447
[b]Wetsus, Centre of Excellence for Sustainable Water Technology, Agora 1, P.O. Box 1113, 8900 CC Leeuwarden, The Netherlands
[c]Université de Rennes 1, CNRS UMR no 6226, Sciences Chimiques de Rennes, Equipe MaCSE, France
[d]Photovoltaic and Optoelectronics Devices Group, Departament de Física, Universitat Jaume I Av Sos Baynat s/n, 12071, Castelló, Spain. E-mail: bisquert@fca.uji.es; Fax: +34 964729218; Tel: +34 964387554

oxidation of organic materials in the anode, resulting in the release of electrons. These electrons flow to the cathode, where usually, oxygen is reduced to water. The latest advances in anodic electrocatalysis and material development for enhanced MFC operation have been recently reviewed in Qiao *et al.*[2] During the past few years, the performance of MFCs in terms of current density and power density has considerably improved. Although oxygen is the preferred electron acceptor at the cathode, it has become clear that the reaction rate for oxygen reduction at the cathode is one of the main limiting factors in MFC performance.[3] Suitable and affordable catalysts are required to overcome this problem. Microorganisms are cheap and renewable catalysts for the cathodic oxygen reduction, leading to the development of oxygen reducing biocathodes.[4–6]

Broader context

We need alternative, renewable energy sources to replace fossil fuels. In the search for renewable energy technologies, microbial fuel cells (MFCs) are a promising option, as they convert biomass into electricity at high energy efficiency, thereby not only producing electricity but also cleaning organic waste streams. The current density and power output of MFCs is currently limited by energy losses at the cathode. To increase the current density and power density to such levels that practical application becomes attractive, cheap and renewable cathode catalysts are required. Biocathodes use the catalytic activity of microorganisms to increase the oxygen reduction rate, and to decrease the energy losses, at the cathode. Insight into the main processes governing biocathode behavior is required to estimate their potential as a renewable cathode catalyst and to provide directions for the improvement of biocathode performance. The use of electrochemical impedance spectroscopy (EIS) is promising as it can be used to distinguish between the different processes that determine biocathode behavior, however, the impedance spectra need careful interpretation using a suitable model in combination with a systematic experimental approach.

This journal is © The Royal Society of Chemistry 2011

Energy Environ. Sci., 2011, **4**, 5035–5043 | 5035

Previous study investigated the performance of three oxygen reducing biocathodes grown at different cathode potentials.[6] These biocathodes consisted of microorganisms originating from nitrifying sludge. The performance of the biocathodes was studied at different linear flow velocities and different cathode potentials. It was shown that both oxygen mass transfer and charge transfer were the main factors limiting the performance of the biocathode.[6] The extent to which both processes limited the biocathode performance, however, has not yet been elucidated. Electrochemical impedance spectroscopy (EIS) is a well-known technique that measures the impedance of a system at different frequencies. The use of EIS in this field may be applied to discriminate and quantify the different processes determining biocathode performance, such as ohmic resistance, charge transfer resistance, diffusion resistance, and capacitance. These processes can be distinguished provided that their characteristic frequencies are sufficiently different. An additional advantage of EIS is that it does not disturb the operation of MFCs at a chosen potential.[7]

In this study, we further analyze the performance of an oxygen reducing biocathode grown in the previous study[6] by using EIS. Our main objective is to identify and quantify the processes limiting the oxygen reduction at the biocathode. Insight into these limitations is required to improve the future design of biocathodes. To gain this insight, we developed a model, required to attribute a specific process to a specific frequency in the EIS spectrum. We validated this model using a systematic experimental approach, where we varied both the electrode potential and the rate of oxygen supply. In order to simplify the set-up as much as possible, we used a flat electrode, enabling the acquisition of impedance spectra under a controlled diffusion layer.

The model description of EIS results for this specific system combines electronic transfer and transport steps, and mass transfer limitations for the final electron acceptor oxygen. These may eventually lead to a complex model combining charge transfer elements and the potential gradient across the film thickness. In the present study, however, we aim for a simple interpretation based on classical reaction–diffusion models that may lay the basis for more detailed studies in the future. From our analysis, we could successfully differentiate between charge transfer and mass transfer limitations.

2. Materials and methods

Electrochemical cell setup

A bio-electrochemical cell was used,[8] containing two flow channels with a projected surface area of 22 cm² and a channel depth of 1.5 cm. The flow channels were separated by a cation exchange membrane (Fumasep FTCM-E, Fumatech, Braunschweig, Germany). The cathode was a rough graphite plate (Al₂O₃ blasted) (Müller & Rössner GmbH & Co, Troisdorf, Germany), while the anode was a flat graphite plate (Müller & Rössner GmbH & Co, Troisdorf, Germany).

Electrochemical cell operation

The catholyte was inoculated with nitrifying biomass from the wastewater treatment plant in Ede, the Netherlands. The cell was

inoculated on day 1 with 100 ml nitrifying biomass, from which the biofilm developed. The catholyte had a total volume of 1 l and consisted of a microbial growth medium of phosphate buffer (pH = 7, 0.02 M), and macro- and micronutrients (10 ml l⁻¹ and 1 ml l⁻¹) as described in Ter Heijne et al.[6] The anolyte also had a total volume of 1 l and was a 0.05 M potassium ferrocyanide solution in 0.02 M phosphate buffer at pH = 7. Ferrocyanide was used as it is a convenient electron donor often used in MFC studies.[9]

The biocathode was started up at a potential of 0.15 V vs. Ag/AgCl. A multi-channel potentiostat (Bank Elektronik—Intelligent Controls GmbH, Pohlheim, Germany) was used. In order to control the cathode potential, a cell voltage was applied between the anode and cathode, and this cell voltage was manually adjusted to the desired cathode potential.[6] This approach was chosen to prevent instabilities in control, e.g. due to defects in the reference electrode, that can be met during long-term experiments. The biocathode produced an average current density of 244 ± 53 mA m⁻² between day 10 and 60. The performance of the biocathode was studied by polarization curves in the previous study.[6] The specific microorganisms catalyzing the reduction of oxygen, and the mechanisms of electron transfer were not studied and identified. After 60 days, the cathode potential was stepwise increased to 0.2 V vs. Ag/AgCl, resulting in a current density of 200 mA m⁻². From day 60 on, EIS measurements were carried out. In between the potentiostatic EIS measurements, the cathode potential was controlled at 0.2 V vs. Ag/AgCl.

The catholyte was actively aerated with air, resulting in an oxygen concentration of 7.5 mg l⁻¹. The catholyte pH was manually controlled at pH = 7 by adding HCl or NaOH. Both anolyte and catholyte were recirculated at a rate of 12 l h⁻¹, except when noted differently. Both anode and cathode compartments were equipped with Ag/AgCl, 3 M KCl reference electrodes (+0.205 V vs. NHE). The cathode potential was measured versus its reference electrodes and recorded every 60 seconds via a Fieldpoint FP-AI-110 module connected to a PC. All experiments were performed inside a temperature controlled chamber at 30 °C.

Electrochemical characterization

Electrochemical impedance of the biocathodes was measured using a potentiostat (IVIUM technologies, Eindhoven, The Netherlands). The potentiostat was connected to the bio-electrochemical cell applying a stationary potential at the cathode compared to the reference electrode, while a small ac signal was used to perturb the system and obtain the impedance spectra.[10] Measurements were taken using the biocathode as the working electrode, an Ag/AgCl (3 M KCl) as reference electrode, and the graphite anode (with ferrocyanide oxidation) as the counter electrode. The cathode was set at the desired potential for 300 seconds before the impedance measurement was started. 51 frequencies were tested, ranging from 10⁴ Hz to 10⁻³ Hz. The amplitude of the applied ac voltage was 10 mV.

The experiments were performed changing the flow rate of the peristaltic pump between 0 and 80 rpm, resulting in a linear flow rate of 0 to 2.8 cm s⁻¹, and at different potentials of 0.18, 0.20, 0.25, 0.28, and 0.35 V vs. Ag/AgCl.

The software used for data fitting was Zview from Scribner Associates Inc. The type of fitting employed was complex (both the real and imaginary impedance values are fit) and the maximum number of iterations for convergence was 100. The error estimation for each parameter was always below 5% for the diffusive components (R_d and ω_d) and below 1% for the pure resistive and capacitive elements (R_s, R_{ct} and C).

3. Results and discussion

Development of the impedance model

Fig. 1(a) shows the polarization curve of the biocathode recorded before the first EIS measurement was started. The maximum current density was 204 mA m^{-2} at an overpotential of 0.6 V ($E_{cat} = 0$ V vs. Ag/AgCl). The polarization curve has the typical S-shape that has been described before for bioanodes.[11,12] For
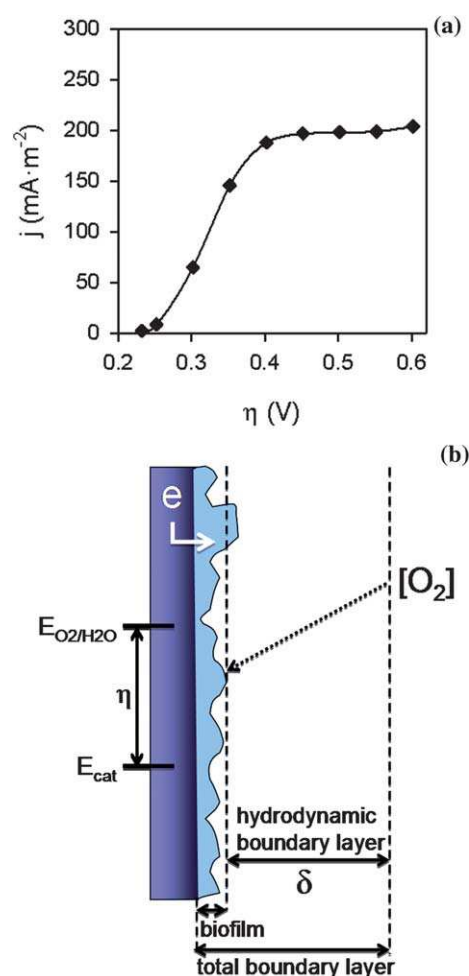

Fig. 1 (a) Polarization curve of the biocathode shows the typical S-shape that has also been observed for bioanodes. The maximum in current density is reached as a result of a maximum in biochemical conversion rate and/or mass transfer limitations. (b) Schematic representation of the biocathode. The electrode is polarized at E_{cat} with an overpotential η compared to the standard potential $E_{O_2/H_2O} = 0.60$ V vs. Ag/AgCl. This results in electron transfer from the electrode to the microorganisms in the biofilm. Oxygen is transported from the bulk solution through the hydrodynamic boundary layer to the biofilm, its concentration decreasing towards the biofilm.

bioanodes, this S-shape is the result of combined electrochemical kinetics, describing the electron transfer from the microorganism to the electrode, and biochemical kinetics, describing the electron transfer from the substrate (organic material) to the microorganism. At low overpotentials (anode potential close to the thermodynamic anode potential), the electrochemical kinetics are dominant, while at high overpotentials, the biochemical kinetics are dominant. In the absence of mass transfer limitations, the maximum in current density can thus be attributed to a maximum in biochemical kinetics, i.e. a maximum in bacterial conversion rate. Bioanode kinetics have been satisfactorily modeled with the Butler–Volmer–Monod model[11] and the Nernst–Monod model.[12]

The exact mechanisms governing the electron transfer steps in biocathodes have not been described in detail, however, a recent review paper[13] shows that the mechanisms for biocathodes are likely to be similar to processes at bioanodes; only the redox potential at which the reactions occur is different. Proposed electron transfer mechanisms for extracellular electron transfer of bioanodes are (i) through direct contact between a single layer of microorganisms and the electrode, (ii) via soluble electron shuttles, and (iii) through a solid conductive matrix.[9] As the mechanisms for biocathodes and bioanodes seem similar, the combination of biochemical and electrochemical kinetics that is characteristic for bioanodes, as described by the Butler–Volmer–Monod model[11] and the Nernst–Monod model,[12] is likely to be similar for biocathodes.

Whereas the maximum current for bioanodes is reached as a result of a maximum in biochemical conversion rate, the situation for biocathodes is different. For biocathodes, we should include diffusion effects as it has been shown that mass transfer limited the maximum current density,[6] which is partly a result of the poor solubility of oxygen compared to e.g. acetate. A simple schematic representation of the biocathode is shown in Fig. 1(b). The overpotential η is the driving force for the electron flow and is defined as the difference between the thermodynamic potential for oxygen reduction ($E_{O_2/H_2O} = 0.60$ V vs. Ag/AgCl) and the cathode potential. Considering mass transfer, the simplest approach is to consider diffusive transport across a boundary layer of thickness δ as indicated in Fig. 1(b). We assume that the thickness of the boundary layer is mainly determined by the hydrodynamic boundary layer, and the contribution of the biofilm to the total boundary layer thickness is minimal.[8] The validity of this assumption is confirmed further on in the text.

Based on these considerations, the EIS response of the oxygen reduction reaction can be described by a standard and quite fundamental model shown in Fig. 2(a) comprising the following elements:

(1) Charge transfer resistance R_{ct} (Ω m^2) that lumps the electron kinetics driven by the overpotential η:

$$R_{ct} = \frac{d\eta}{dj} \qquad (1)$$

where j = current density (A m^{-2}).

(2) A parallel capacitance (CPE). This may represent a double layer capacitance at the film/solution interface, but may also describe electron or ion accumulation phenomena in the biofilm or the substrate.

(3) The finite size diffusion element for transport across a boundary layer of thickness δ (Z_d).
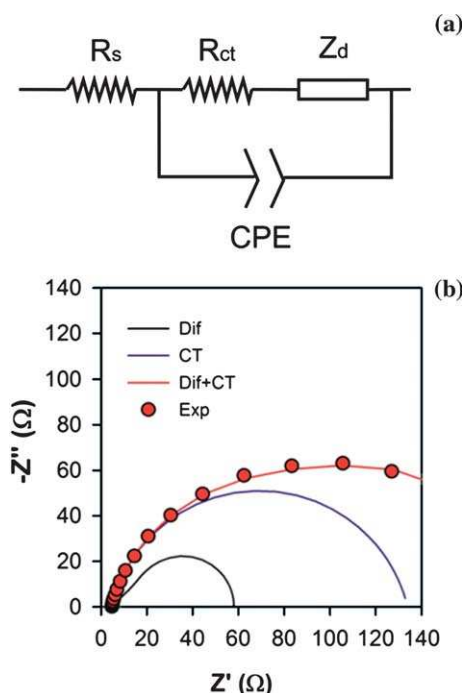
Fig. 2 (a) Generalized Randles equivalent circuit employed to model charge transfer and finite length diffusion Z_d. R_{ct} is the charge transfer resistance and CPE models the interfacial capacitance. (b) Fit of the experimental data to the model. The points are the experimental EIS data at $E_{cathode} = 0.28$ V $vs.$ Ag/AgCl and flow rate 2.8 cm s^{-1}. The line is a fit to the data, and two different contributions to the impedance are separately shown: the diffusion impedance (Dif) and charge transfer elements (CT).

(4) A series resistance for ohmic transport in the electrolyte and other contact effects (R_s).

Therefore, the model to describe our EIS results is a generalized Randles circuit with a finite length Warburg element for the diffusion transport of reactant to the reacting surface. A finite length Warburg element was used following the same approach found in the literature for modeling the oxygen evolution reaction, for example in solid ionic conductor La$_{1-x}$Sr$_x$CoO$_{3-d}$,[14] and PEM fuel cells.[15]

The diffusion impedance Z_d (Ω m^2) can be written as:

$$Z_d = R_d \frac{\tan h(i\omega/\omega_d)^{1/2}}{(i\omega/\omega_d)^{1/2}} \quad (2)$$

where $i = \sqrt{-1}$, ω is the frequency (s^{-1}), ω_d is the diffusion frequency, related to the diffusion coefficient D (m^2 s^{-1}) through

$$\omega_d = \frac{D}{\delta^2} \quad (3)$$

where δ the boundary layer thickness (m) and, finally, the diffusion resistance R_d (Ω m^2) can be expressed as:

$$R_d = \frac{\delta}{FaD} \left(\frac{dE}{d[O_2]} \right)_{\overline{E}} \quad (4)$$

where Fa = Faraday constant (C mol^{-1}), $(dE/dc)_E$ is the slope of the coulometric titration curve, and [O$_2$] is the oxygen concentration (mol m^{-3}).

From eqn (4), the diffusion resistance can be expressed as:

$$R_d = \frac{1}{FaD^{1/2}\omega_d^{1/2}} \left(\frac{dE}{d[O_2]} \right)_{\overline{E}} \quad (5)$$

Therefore, the diffusion resistance correlates with the diffusion frequency as:

$$R_d = B\omega_d^{-1/2} \quad (6)$$

where

$$B = \frac{1}{FaD^{1/2}} \left(\frac{dE}{d[O_2]} \right)_{\overline{E}} \quad (7)$$

Since both mass transport and charge transfer are driven by the overpotential, the charge transfer resistance (R_{ct}) is connected in series with the finite length Warburg element in Fig. 2 (a). A constant phase element (CPE) accounting for interfacial capacitance is connected in parallel. The impedance of the constant phase element is described by two parameters, Q and n, as:

$$Z_{CPE} = \frac{1}{Q(i\omega)^n} \quad (8)$$

where Q has dimension of F s^{n-1}, and n is an adimensional parameter accounting for non-ideal behavior. The interfacial capacitance C is calculated as:[16]

$$C = R_{ct}^{(1-n)-1} Q^{1/n} \quad (9)$$

Fig. 2(b) shows an example of fitting for our results, and the contribution of the separate components: the diffusion impedance and charge transfer elements (an arc in the complex plot). In general, these two elements may appear clearly differentiated in the experimental data (as within the above references), or closely convoluted. This depends on the relative values of resistances or capacitances. If the diffusion resistance is smaller than the charge transfer resistance, we may have both contributions mixed in the spectra and the characteristic 45° line of diffusion is not visible, as observed in Fig. 2(b). In this situation, the impedance model must be validated by the judicious analysis of the parameters extracted from the fitting process.

Analysis of mass transfer effects at constant potential

The impedance spectra were first measured at constant potential and at different flow rates. Fig. 3(a) shows the Nyquist plots obtained at a cathode potential of 0.28 V $vs.$ Ag/AgCl. The variation in the impedance curves for the different flow rates is a clear indication that diffusion plays a predominant role in the behavior of the biocathode. Fig. 3(b) summarizes the parameters R_{ct} and R_d obtained from fitting the impedance data using the model indicated in Fig. 2(a). The results show that R_{ct} does not significantly change with the flow rate (except at 0 cm s^{-1}), and the main variation in resistance comes from diffusion (R_d). This result is fully consistent with our model as R_{ct} is governed by the overpotential, which remains unchanged, while R_d changes, as ω_d is affected by the flow rate through δ (eqn (3)). The result at 0 cm s^{-1} is associated with the large error found in the fit of the parameter at this condition, where the resistance is largely dominated by diffusion.
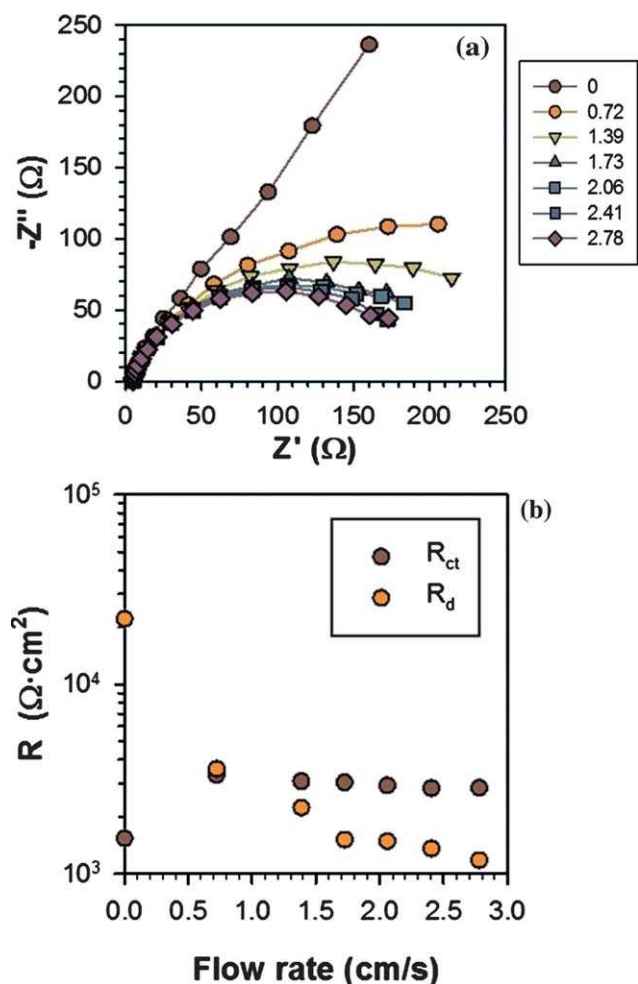
Fig. 3 (a) Nyquist plots obtained for the biocathode at different flow rates (expressed in cm s⁻¹) and constant cathode potential of 0.28 V *vs.* Ag/AgCl. (b) R_{ct} and R_d resulting from the fit with the model.

Another important element which can be analyzed from the mass transfer EIS experiments is the interfacial capacitance. This capacitance was obtained from fitting the experimental data to the model in Fig. 2(a) and subsequently by applying eqn (9). The capacitance was found to be fairly constant for the different flow rates, as expected for an interfacial capacitance. However, the obtained values (around 1 mF cm⁻²) measured for these bio-cathodes are extremely high for an interfacial capacitance. The usual specific capacitance associated with the Helmholtz layer is around 10 μF cm⁻².[17] A capacitance 100 times larger may have several origins associated with a certain charge storage phenomenon in the electrode or biofilm, such as a redox[18] or chemical capacitance.[19] It may indicate either electron accumulation in the biofilm (the bacteria can store electrons in their surface or in their own cells) or proton insertion into the graphite cathode, which is the standard mechanism of capacitance in battery intercalation materials.[20]

The same behavior reported for $V_{cathode} = 0.28$ V has been observed for the different tested potentials between 0.15 and 0.35 V *vs.* Ag/AgCl. When diffusion was not considered in the model ($Z_d = 0$ in the model of Fig. 2(b)), it was observed that the interfacial capacitance (C) decreased with increasing flow rate

(not shown). This behavior is inconsistent, since the capacitance should be independent of flow rate and it is a property of the combined electrode and biofilm. This is another indication that diffusion is an essential element to be included in the model. It is important to emphasize that good numerical agreement between model fitting and experimental data does not justify the validity of the selected model, since a good correspondence can be also obtained using different models. This fact underlines that the validity of the employed model cannot be deduced from the numerical agreement of experimental data and equivalent circuit, but from the physical interpretation of the extracted parameters.

Validating the model by determining the boundary layer thickness

A useful strategy to validate the impedance model is to calculate a common parameter by different procedures. For instance, we can calculate the boundary layer thickness from (i) the EIS results, using eqn (3), and from (ii) the linear diffusion model[21] as described in Ter Heijne et al.[8] This linear flow model can be used to calculate the average mass transfer rate in the reactor[21] *via* the following equations:

$$Pe = \frac{D_T \nu}{D} \quad (10)$$

$$Sh = 3.66\left(1 + 0.095\frac{D_T}{L}Pe\right)^{0.45} \quad (11)$$

$$Sh = \frac{kD_T}{D} \quad (12)$$

$$\delta = \frac{D}{k} \quad (13)$$

where Sh = Sherwood number, D_T = hydraulic diameter = 2WH/(W + H) (W = width = 2.0 cm, H = height = 1.5 cm), L = channel length = 12 cm, Pe = Peclet number, ν = flow velocity, D = diffusion coefficient for oxygen in water = 2×10^{-5} cm² s⁻¹,[22] k = mass transfer coefficient, and δ = boundary layer thickness.

Following the linear flow model, the thickness of the boundary layer was calculated as a function of flow rate *via* the Peclet number Pe (eqn (10)). The Peclet number was used to calculate the Sherwood number Sh (eqn (11)), from which the mass transfer coefficient k (ms⁻¹) was determined (eqn (12)).[8] Finally, the boundary layer thickness was calculated from the mass transfer coefficient *via* eqn (13). This calculated boundary layer was increased by 56 μm, to take into account the stagnant water layer attached to the biofilm that cannot be influenced by the recirculation rate.[6,23] This resulted in a boundary layer thickness ranging from 299 μm (for 0.36 cm s⁻¹) and 106 μm (for 3.6 cm s⁻¹) (Fig. 4(a)). An excellent agreement was found between both procedures (Fig. 4(a)), using $D = 2 \times 10^{-5}$ cm² s⁻¹ for the effective diffusion coefficient of oxygen in water (identical to the linear flow model), and eqn (3) to calculate the thickness of the boundary layer. This further validates the applicability of our EIS model.

Biofilms observed so far in MFCs are thin, ranging from a monolayer[24] to about 40 μm thickness.[25] Consequently, with the values obtained for δ between 106 and 299 μm, we can safely
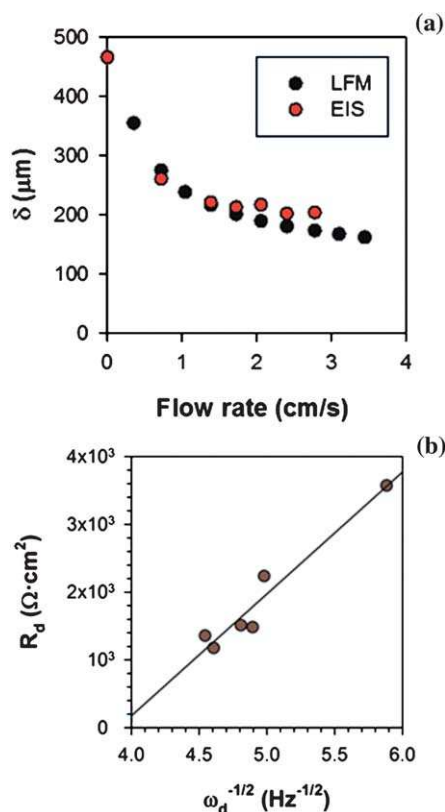
Fig. 4 (a) Effective diffusion length calculated from EIS (eqn (3)) and from the linear flow model (eqn (9)–(12)) taking the effective diffusion coefficient for oxygen in water: $D = 2 \times 10^{-5}$ cm² s⁻¹.[22] (b) Diffusion resistance R_d vs. $\omega_d^{-1/2}$ are linearly related, as expected from eqn (6). Results are obtained from fitting the spectra of Fig. 3(a) to the model.

assume that it is mainly the hydrodynamic boundary layer, and not the biofilm, which determines the effect of mass transfer limitations on the current density.[8]

The validity of our model was further confirmed by analysis of the diffusion frequency. This showed an increase in ω_d with flow rate, reflecting the decrease in the boundary layer thickness (see eqn (3)), related to improved mass transfer of oxygen. Besides, a linear relationship was found between R_d and $\omega_d^{-1/2}$, as expected from eqn (6) (Fig. 4(b)).

Analysis of mass transfer and charge transfer effects at constant flow rate

To gain further insight into the rate-limiting processes governing the maximum in current density observed in the polarization curve (Fig. 1(a)), we analyzed the EIS results obtained under conditions of constant flow velocity (2.1 cm s⁻¹) and at different cathode potentials in the range between 0.18 and 0.35 V vs. Ag/AgCl. The obtained Nyquist plots are shown in Fig. 5(a). The values for the parameters R_{ct} and R_d are shown together with R_{tot}, calculated as $R_{tot} = R_{ct} + R_d + R_S$ (Fig. 5(b)). For comparison, R_{tot} was also calculated from the derivative of the polarization curve (Fig. 1(a)).

An excellent agreement (12–45% relative difference) was found between the values for R_{tot} from EIS and from the polarization curve. Fig. 5(b) shows a minimum in R_{tot} at $E = 0.28$ V vs. Ag/AgCl. This minimum in R_{tot} is dominated by R_{ct}. The observed
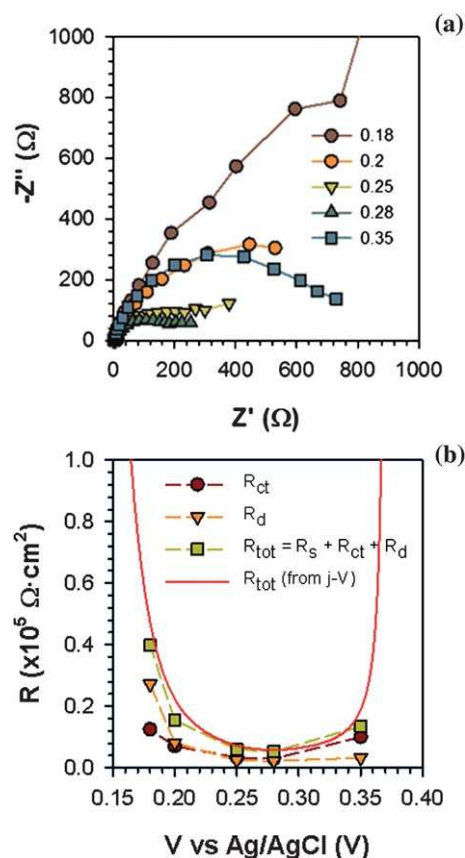

Fig. 5 (a) Nyquist plots at constant flow rate (2.1 cm s⁻¹) and different cathode potentials (expressed as V vs. Ag/AgCl). (b) R_{tot}, R_{ct} and R_d resulting from the fit with the model, and from the slope of the polarization curve (as shown in Fig. 1(b)). Dashed lines are plotted as a guide for the eye.

behavior of R_{ct}, now decoupled from diffusion effects, can be understood using the previously developed bioanode models. As indicated above, two different processes contribute to the measured R_{ct} in the system: (i) the electron transfer from the biofilm to the electron acceptor (oxygen), and (ii) the biochemical reactions occurring at the enzymatic centers within the microbial cell. At low overpotentials (high cathode potentials), the electron transfer reaction is limiting and an increase in overpotential will lead to an increase in electron transfer rate and decrease in the charge transfer resistance. At higher overpotentials (lower cathode potentials), however, the biochemical reactions that determine the rate of electron transfer from the bacterial cell to oxygen become rate limiting. Since the rate of these biochemical reactions is not influenced by an increase in overpotential but by the concentration of oxidized and reduced species of the redox component involved in electron transfer, a further increase in overpotential will not lead to an increase in current. This implies that the charge transfer resistance will rise again at higher overpotentials. This is an important difference between combined biochemical and electrochemical kinetics, and electrochemical kinetics alone. The minimum in the charge transfer resistance is thus a result of the occurrence of biochemical reactions that become limiting at higher overpotential.

From Fig. 5(b) we see that the charge transfer resistance was a factor 1.4 higher than the diffusion resistance in the vicinity of

5040 | Energy Environ. Sci., 2011, 4, 5035–5043

This journal is © The Royal Society of Chemistry 2011

$E = 0.28$ V *vs.* Ag/AgCl. Therefore, the reaction rate at this potential was not limited by diffusion but by charge transfer. Conversely, at the higher overpotentials tested, R_{ct} became smaller than R_d, and the diffusion resistance was dominant. This result indicates that not only biochemical kinetics (included in R_{ct}) are responsible for the limited current at high overpotentials, as dictated by Monod kinetics, but also diffusion controls the response of the biocathode: the diffusion resistance increases with decreasing cathode potential and is dominant at high overpotentials. The high current generation at low cathode potential requires a faster transport of oxygen, causing an increased diffusion resistance.

The combined effect of mass and charge transfer resistances is responsible for the S-shaped polarization curve shown in Fig. 1 (a), which is typical for electrochemically active bacteria. The result justifies that diffusion is essential to be taken into account for an accurate and detailed investigation of the kinetics of the biocathode, although the potential dependence of R_{ct} alone also produces an S-shaped polarization curve.

The calculated values for capacitance were practically identical to those obtained for the different flow rates (1 mF cm^{-2}), which further validates our analysis. These results are in good agreement with those obtained from cyclic voltammetry (CV) experiments,[5] calculated as $C = j_{cap}/s$ where j_{cap} is the capacitive current on top of the diffusion-limited current, and s is the scan rate. Based on these CV data, a capacitance between 1 and 2 mF cm^{-2} was found, which is similar to the interfacial capacitance determined from EIS. *Via* both methods, it was found that the capacitance is nearly constant with a slight increase with the cathodic potential. From this behavior, it is not possible to conclude the specific origin of the capacitance. The electrons likely follow a chain of redox components between the electrode and oxygen. These different redox components provide an electron storage capacity, each at their specific potential, which can result in the measured capacitance. When multiple redox centers are present with different standard potentials, the resulting capacitance is less dependent on the potential, as the faradaic peaks overlap. Further investigation is needed to elucidate the exact mechanisms that contribute to the capacitance.

Butler–Volmer–Monod model predicts minimum in R_{ct}

Using EIS, we could quantitatively analyze the contribution of charge transfer and mass transfer resistances to the total internal resistance. To further validate this analysis, we used the Butler–Volmer–Monod model, including mass transfer, to predict the observed trends in R_{ct} and R_d.

The steady-state solution of the Butler–Volmer–Monod model[11] expresses the current density j as a function of overpotential η and oxygen concentration $[O_2]$ according to:

$$\frac{j}{j_{max}} = \left(\frac{1 - e^{-f\eta}}{K_1 e^{-(1-\alpha)fn} + K_2 e^{-fn} + 1} \right) \times$$

$$\left(\frac{[O_2]}{(K_M/K_1 e^{-(1-\alpha)fn} + K_2 e^{-fn} + 1) + [O_2]} \right) \quad (14)$$
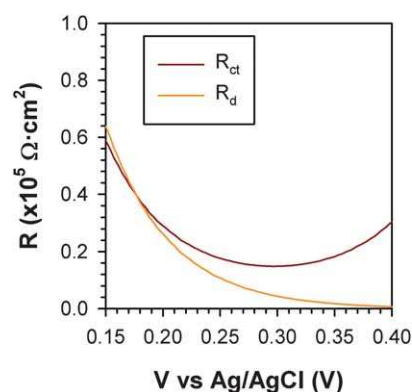

Fig. 6 The Butler–Volmer–Monod model predicts similar trends in R_{ct} and R_d as observed from the EIS analysis (compare with Fig. 5(b)).

where j_{max} = maximum current density (A m^{-2}), $f = F/RT$ (V^{-1}), K_1 and K_2 = dimensionless lumped parameters (see below), K_M = affinity constant for oxygen (mol m^{-3}).

The charge transfer and diffusion resistances are described by eqn (1) and (4). Using the Butler–Volmer–Monod model, we could simulate the trends in R_{ct} and R_d using the following parameter values: $\alpha = 0.5$, $j_{max} = 0.2$ A m^{-2}, $K_1 = 50$, $K_2 = 15$, and $[O_2] = 3K_M$. The validity of these assumptions can be checked when we consider the meaning of the parameters. K_1 can be interpreted as the ratio between the rate of the biochemical reaction compared to the electrochemical reaction. As chemical oxygen reduction at pH 7 is a kinetically slow reaction, we can safely assume that the electrochemical rate is small compared to the biochemical rate, *i.e.* one would expect that $K_1 \gg 1$. K_2 can be interpreted as the ratio of the forward reaction from a redox component complex to product (water) over the backward reaction of the redox component to the substrate (oxygen). As the microorganisms gain energy from converting the substrate into product, $K_2 \gg 1$. The ratio $[O_2]/K_M$ determines to what extent the oxygen concentration limits the current density. As mass transfer is clearly affecting biocathode performance, the ratio should be low.

Using these parameters, we calculated R_{ct} and R_d as a function of overpotential. The result is shown in Fig. 6. The trends in R_{ct} and R_d as a function of overpotential are similar to the results obtained by fitting our impedance results to the standard model (Fig. 5(b)). We see that the Butler–Volmer–Monod model predicts a similar minimum in R_{ct}, and a similar increase in R_d with decreasing potential. This analysis shows that the combined biochemical and electrochemical kinetics, which is the basis of the Butler–Volmer–Monod model, indeed result in a minimum in R_{ct}. Furthermore, the Butler–Volmer–Monod model describes the processes governing biocathode behavior well. Further study combining EIS results with the Butler–Volmer–Monod model may be used to estimate the kinetic parameters determining biocathode performance.

Implications

In this study, we analyzed the factors limiting biocathode performance by EIS. Our interpretation based on classical reaction–diffusion models may lay the basis for more detailed studies in the future. Suggested points to improve our understanding of the functioning of a biocathode are the following:

(a) To identify the origin of the large specific capacitance. Several possibilities have been mentioned above: the redox capacitance as in conductive polymer films, or an insertion capacitance. In order to clarify this issue, control experiments may be needed in which charge-transfer is suppressed, and the capacitance is investigated over a wide voltage range in different electrolyte conditions.

(b) Insight into bioelectrochemical kinetics in the biofilm. If the overall impedance model is well resolved in a variety of situations, it may be possible for EIS results to resolve separate elements of the enzyme kinetics and electron transfer reactions.

(c) Investigation of the electrode morphology. The literature indicates several mechanisms whereby the enzymatic centres communicate with the electrode, either by direct electron transfer, *via* a redox shuttle, or in a solid conductive matrix.[9] In the case of a relatively thick biofilm, the oxygen diffusion or electron transport across the biofilm is not facile and should produce a combination of a gradient of the reacting species (oxygen) and a gradient of the overpotential across the biofilm, as transport and reaction are coupled, in addition to an external diffusion layer. A more extensive model could help elucidating these mechanisms.

Our impedance results as shown in the Nyquist plots showed an arc almost in all cases. No typical 45° Warburg line, representing diffusion limitations, was generally observed (except for Fig. 3(a) at 0 cm s^{-1} and at 0.18 V *vs.* Ag/AgCl in Fig. 5(a)). In case no Warburg line is observed, the arc is usually interpreted *via* a Randles circuit, disregarding mass transport limitations. When increasing the flow rate, however, we found that the size of the arc decreased, indicating that mass transfer did play a dominant role. Including a diffusion resistance in the standard model gave consistent results. In order to correctly interpret EIS results involving microbial electrodes, it is thus recommended to include measurements under different mass transfer conditions. Also, measurements at different cathode potential and constant mass transfer conditions are useful to study charge transfer processes. Furthermore, with the model used in this study, we were able to distinguish between diffusion resistance and charge transfer resistance. Consequently, EIS has proved to be a useful tool for in-depth analysis of the biocathode behavior.

The EIS results show that, depending on the flow rate, the diffusion resistance largely determines biocathode performance. At a cathode potential of 0.18 V *vs.* Ag/AgCl, the diffusion resistance was a factor 2.2 higher than the charge transfer resistance. To decrease the diffusion resistance and improve mass transfer of oxygen, the use of air cathodes is recommended.[6] Besides a reduction in diffusion resistance, a reduction in charge transfer resistance will be needed to obtain higher current densities. Ways to decrease the charge transfer resistance would be to increase the specific surface area of the electrode, *e.g.* by using porous electrodes, and to optimize the process conditions and the biofilm composition. For this, characterization of the microorganisms responsible for the catalysis of oxygen reduction could be helpful.

Conclusions

We characterized the electrochemical behavior of the biocathode of a microbial fuel cell by impedance spectroscopy. For meaningful interpretation of impedance spectra, a suitable model is required, and to be able to distinguish between the limiting processes, the characteristic frequency for each process should be different. The obtained impedance spectra could be interpreted with standard charge transfer resistance, a finite length diffusion impedance, and a parallel capacitance. In general, charge transfer and diffusion impedance appear clearly differentiated in the experimental data, or closely convoluted, depending on the relative values of resistances or capacitances. We found both contributions mixed in the spectra, so that the characteristic 45° line of diffusion was not visible in most cases. Therefore, we validated the impedance model by measurements under a controlled diffusion layer and controlled cathode potential.

Acknowledgements

References

1 B. E. Logan, B. Hamelers, R. Rozendal, U. Schröder, J. Keller, S. Freguia, P. Aelterman, W. Verstraete and K. Rabaey, *Environ. Sci. Technol.*, 2006, **40**, 5181–5192.

2 Y. Qiao, S.-J. Bao and C. M. Li, *Energy Environ. Sci.*, 2010, **3**, 544–553.

3 H. V. M. Hamelers, A. Ter Heijne, T. H. J. A. Sleutels, A. W. Jeremiasse, D. P. B. T. B. Strik and C. J. N. Buisman, *Appl. Microbiol. Biotechnol.*, 2010, **85**, 1673–1685.

4 P. Clauwaert, D. Van Der Ha, N. Boon, K. Verbeken, M. Verhaege, K. Rabaey and W. Verstraete, *Environ. Sci. Technol.*, 2007, **41**, 7564–7569.

5 S. Freguia, S. Tsujimura and K. Kano, *Electrochim. Acta*, 2010, **55**, 813–818.

6 A. Ter Heijne, D. P. B. T. B. Strik, H. V. M. Hamelers and C. J. N. Buisman, *Environ. Sci. Technol.*, 2010, **44**, 7151–7156.

7 Z. He and F. Mansfeld, *Energy Environ. Sci.*, 2009, **2**, 215–219.

8 A. Ter Heijne, H. V. M. Hamelers, M. Saakes and C. J. N. Buisman, *Electrochim. Acta*, 2008, **53**, 5697–5703.

9 C. I. Torres, A. K. Marcus, H. S. Lee, P. Parameswaran, R. Krajmalnik-Brown and B. E. Rittmann, *FEMS Microbiol. Rev.*, 2010, **34**, 3–17.

10 D. P. B. T. B. Strik, A. Ter Heijne, H. V. M. Hamelers, M. Saakes and C. J. N. Buisman, *ECS Trans.*, 2008, **13**, 27–41.

11 H. V. M. Hamelers, A. ter Heijne, N. Stein, R. A. Rozendal and C. J. N. Buisman, *Bioresour. Technol.*, 2011, **102**, 381–387.

12 C. I. Torres, A. K. Marcus, P. Parameswaran and B. E. Rittmann, *Environ. Sci. Technol.*, 2008, **42**, 6593–6597.

13 M. Rosenbaum, F. Aulenta, M. Villano and L. T. Angenent, *Bioresour. Technol.*, 2011, **102**, 324–333.

14 S. B. Adler, *Solid State Ionics*, 1998, **111**, 125–134.

15 X. Yuan, H. Wang, J. C. Sun and J. Zhang, *Int. J. Hydrogen Energy*, 2007, **32**, 4365–4380.

16 J. Bisquert and F. Fabregat-Santiago, in *Dye-Sensitized Solar Cells*, ed. K. Kalyanasundaram, CRC Press, Boca Ratón, 2010, ch. 12, pp. 457–555.

17 A. J. Bard and L. R. Faulkner, *Electrochemical Methods, Fundamentals and Applications*, John Wiley & Sons, Weinheim, 2nd edn, 2001.

18 C. E. D. Chidsey and R. W. Murray, *J. Phys. Chem.*, 1986, **90**, 1479–1484.

19 J. Bisquert, *Phys. Chem. Chem. Phys.*, 2003, **5**, 5360–5364.

20 M. D. Levi, E. A. Levi and D. Aurbach, *J. Electroanal. Chem.*, 1997, **421**, 89–97.

21 R. E. Hayes and S. T. Kolaczkowski, *Chem. Eng. Sci.*, 1994, **49**, 3587–3599.

22 C. Picioreanu, M. C. M. Van Loosdrecht and J. J. Heijnen, *Water Sci. Technol.*, 1997, **36**, 147–156.

23 K. Williamson and P. L. McCarty, *J. - Water Pollut. Control Fed.*, 1976, **48**, 9–24.

24 D. R. Bond and D. R. Lovley, *Appl. Environ. Microbiol.*, 2003, **69**, 1548–1555.

25 G. Reguera, K. P. Nevin, J. S. Nicoll, S. F. Covalla, T. L. Woodard and D. R. Lovley, *Appl. Environ. Microbiol.*, 2006, **72**, 7345–7348.

This journal is © The Royal Society of Chemistry 2011

Energy Environ. Sci., 2011, **4**, 5035–5043 | 5043